### **CONFERENCE PRE-PRINT**

# ACHIEVING LOW-VELOCITY FULL COVERAGE OF GAINSN LIQUID METAL FIRST WALL FILM FLOW BY STRUCTURAL INNOVATION

Y.M. WANG, X.J. Zhang, Y. Zhao, Z.C. Sun, L.Wang, X.T. Lv Southwestern Institute of Physics Chengdu, People's Republic of China Email: wangym@swip.ac.cn

### Abstract

Employing flowing renewable liquid metal as the first-wall material in fusion reactors demonstrates significant advantages including the absence of thermal stress, resistance to neutron irradiation damage, unlimited service lifetime, recyclability, and high steady-state thermal load capacity, thereby providing innovative solutions for DEMO first-wall. However, resolving the MHD instability of liquid metals and achieving full-coverage, stable, and uniform flow under strong magnetic fields remain critical challenges for liquid metal applications. This study employs a combined approach of simulation and experimentation to analyze the effects of magnetic field strength, flow velocity, chute angle and innovative bottom wall structures on the spreading characteristics, aiming to find a way to achieve full coverage of liquid metal GaInSn film flow under a low Re and a poor wetting condition. By comparing the simulation and experimental results, the reliability of the simulation results was verified. The main conclusions are as follows: (a)The coverage area of the film flow first increases and then decreases as the inclination angle of the chute increases from 0° to 90°. The chute angle for maximum GaInSn film flow spreading area is around 30°; (b) Preliminary full-coverage film flow without a magnetic field can be achieved through structural innovation, although further research is needed to assess the spreading behavior of the new bottom wall structure under magnetic field.

### 1. INTRODUCTION

One of the main challenges in future fusion power reactors such as DEMO is managing high heat flux and controlling impurities under quasi-steady or true steady-state operation. The steady-state heat-handling capability of current divertor designs using solid high-Z metal plasma-facing components (PFCs) such as tungsten (W) is limited to approximately 5-15 MW/m<sup>2</sup> [1], which is insufficient to meet DEMO requirements. In addition, neutron irradiation damage is a serious concern, as long-term exposure to 14.1 MeV neutrons degrades the structural strength and thermal conductivity of materials[2]. A promising solution is to replace traditional solid tungsten materials with liquid metals (LMs)[3]. LM can be a long lifetime PFCs, due to its reduced sensitivity to neutron damage, high heat flux handling capability, superior resilience to transients events such as edge localized mode (ELM), and ability to remove impurities, and control of particles recycling. The damaged surface material can self-heal and self-replenish via liquid convection. Moreover, flowing LM not only can remove the high heat and particle fluxes, but also protect the underlying solid substrates[4][5]. The heat load on the PFCs surface and generated impurities can be transported to external systems for regeneration through the circulating LMs[6]. However, as good electrical conductors, LMs are strongly influenced by magnetohydrodynamic (MHD) effects arising from interactions of the induced electric currents with the strong magnetic field to confine fusion plasmas[7]. Therefore, achieving stable and full-coverage spreading of LMs on substrate materials represents the first step toward the application as PFCs.

Experimental and simulation results of the film flow have shown that increasing the inlet flow velocity can expand the spreading area. For example, Stable coverage of the liquid Galinstan (GaInSn) metal flow on the substrate material can only be achieved when the Reynolds number reaches above 20 000 (flow rate: 357.6 cm³/s) [8]. However, spreading LM by increasing the flow rate requires a high-capacity pump system, which poses engineering challenges [8][9]. With advancements in metal 3D-printing methods, capillary porous systems (CPS) with complex capillary channels have been proposed and tested in various plasma devices [10][11]. In comparing experiments with tungsten meshes, tungsten fiber mats, and tungsten sintered disks, tungsten capillary plates have shown their effectiveness in withstanding plasma pulses and enduring higher heat flux densities without surface damage or particle ejection. However, it is important to note that CPS differs from the free surface film flow system. The CPS continuously pumps liquid outward through numerous holes dispersed across the backing plate. Driven by capillary forces, liquid metal climbs within the channels and spreads outwards upon reaching the upper surface of the plate to wet its surrounding area. If the capillary channels become obstructed by impurities from the filtering process, the CPS will lose its protective layer of liquid metal[12]. Numerous studies have also been dedicated to improving the wettability of liquid metals on the substrate materials through surface treatments, such as laser ablation, baking, glow discharge cleaning, and

evaporated lithium coatings [13][14][15]. However, the surfaces after such treatments may changes during use, leading to a reduction in wettability, which in turn necessitates repeated surface treatments.

In this study, numerical and experimental investigations on GaInSn film flows are carried out to study the effects of magnetic field strength, flow velocity and chute angle on the film flow under poor wetting conditions. Then two innovative structural designs are further developed and verified by simulation that long-distance, full-coverage LM GaInSn film flow can be successfully achieved under Re<20000 and poor wetting condition.

### 2. METHODOLOGY

### 2.1. Experiment setup

An experiment on a Galinstan film flow over a flat bottom surface was conducted in the LM MHD experimental loop at Southwestern Institute of Physics (see FIG.1 (a)). The LM is accelerated by two electromagnetic (EM) pumps and flows along the +Y-axis in the free surface test section. The mean flow velocity is measured by an EM flow-meter. To distinguish the EM force from gravity, the test chamber was inclined at an angle of 30° with respect to the horizontal plane(β). The uniform magnetic field cover a region of 80 mm (X direction)×740 mm (Y direction)×170 mm (Z direction). The gradient steady-state magnetic field is controlled by a DC electromagnet power supply and adjusted to the required value. The whole loop is filled with argon to protect GaInSn from oxidation[17]. The free surface liquid test section (see FIG.1 (b)) is composed of 304 stainless steel, a transparent window made of organic glass and nozzle components, etc. During the experiment, the liquid metal is first pressed into the tank, and then electromagnetic pumps are used to drive the circulation of the liquid metal. A liquid free surface is formed through the nozzle. During operation, the pressure of Ar gas in the loop is 0.02 MPa. The MHD effect characteristics of the free surface are recorded by digital pictures and digital videos. The film flow thickness is measured using the Keyence LJ-X8000 line laser measuring instrument. Its measurement principle is as follows: a cylindrical objective lens diffuses the laser into a line laser, which is then projected onto the surface of the target object to form diffuse reflection. The reflected light is imaged on the CMOS, and the displacement and shape are measured by detecting changes in position and shape.

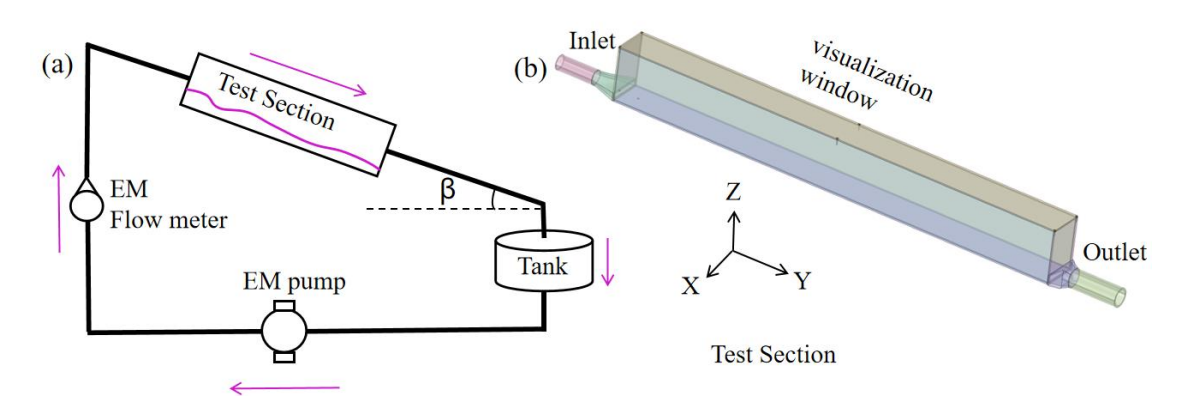


FIG. 1. Sketch of Liquid Metal MHD experimental loop.

### 2.2. Mathematical modeling

The LM free surface film flowing along a chute is illustrated in FIG. 2. The chute is inclined and the angle with respect to the horizontal direction plane is defined as  $\beta$ . The LM flows along Y-direction. In FIG. 2, W denotes the chute width ,  $d_0$  represents the initial film thickness, and  $d_s$  is the local film thickness which varies with the flow distance.

# [Left hand page running head is author's name in Times New Roman 8 point bold capitals, centred. For more than two authors, write

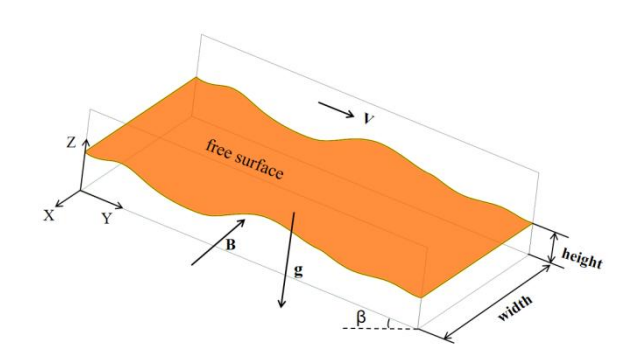


FIG. 2. Sketch of liquid metal flows along a chute.

The governing equations for this two-phase free surface film flow are given in equations (1) and (2), representing the mass conservation and momentum conservation respectively. The variables of  $\rho$ ,  $\vec{V}$ , p, T,  $\vec{g}$ and u correspond to fluid density, the velocity, the pressure, the temperature, the gravity and the dynamic viscosity, respectively.

$$\frac{\partial}{\partial t}(\rho) + \nabla \cdot (\rho \vec{V}) = 0 \tag{1}$$

$$\frac{\partial}{\partial t}(\rho \vec{V}) + \nabla \cdot (\rho \vec{V} \vec{V}) = -\nabla p + \nabla \cdot (\mu(\nabla \vec{V} + \vec{V}^T)) + \rho \vec{g}$$
(2)

Numerical simulations were carried out using FLUENT software. Volume of fluid (VOF) modeling was selected for free surface treatment, as it can represent two or more immiscible fluids by solving a single set of momentum equations while tracking the volume fraction of each fluid throughout the computational domain. In the VOF method, for each additional phase, a variable  $\alpha_q$  is introduced to denote the volume fraction of the  $q_{th}$ phase. Within each control volume, the sum of all  $\alpha_q$  values equals unity. If  $\alpha_q=0$ , the computational cell contains no fluid of that phase; if  $\alpha_q=1$ , the cell is fully occupied by that phase; and if  $0<\alpha_q<1$ , the cell contains an interface between phases. A second-order upwind differencing scheme was used to solve the momentum and continuity equation for the volume fraction function. Pressure-velocity coupling was handled with the PISO algorithm, and the PRESTO method was applied for pressure interpolation. To maintain consistency with the experiment, the chute inclination angle  $\beta$  (FIG. 2) was set to 30°. The contact angles  $\theta$ w was set to 135°, representing poor wettability between the fluid and the solid wall. A velocity inlet was specified as the inlet boundary condition, while a pressure outlet condition was applied at the outlet. A no-slip boundary condition was imposed at all walls.

### RESULTS AND DISCUSSION

### 3.1. Film flow experiment results

Film flow experiments were conducted under varying GaInSn inlet velocities and transverse magnetic field strengths. The primary dimensionless parameters considered were the Reynolds number (Re) and the Hartmann number (Ha). The Reynolds number is defined as Re=Q/v, where Q is the volumetric flow rate, v is the kinematic viscosity (2.98×10<sup>-7</sup> m<sup>2</sup>/s) and w is the flow width (70mm). Different inlet flow velocities were obtained by adjusting the frequency of the EM pump. The corresponding relationship between EM pump frequency, inlet flow velocity and Re is summarized in the table below.

TABLE 1. CORRESPONDING RELATIONSHIP BETWEEN ELECTROMAGNETIC PUMP FREQUENCY (HZ), FLOW VELOCITY (M/S) AND REYNOLDS NUMBER

EM pump frequency (Hz)	Inlet velocity (m/s)	Re
4.5	0.051	1698
5	0.130	4361
5.5	0.256	8589

6	0.313	10503
6.5	0.396	13283
7	0.433	14526
7.5	0.533	17885
8	0.598	20074
8.5	0.662	22205
9	0.676	22671

As shown in FIG.3, in the absence of a magnetic field, the spreading area of the film flow increases with the increase of Re. When Re<13283, liquid GaInSn flow exhibits a narrow rivulet-like pattern, detaching from the sidewalls, failing to spread fully. When Re=14526, a preliminary large-area full coverage of the GaInSn on the bottom stainless-steel wall can be achieved, however, this fully covered state is unstable and a transient exposure of the bottom wall will occur. When Re>20074, a stable full coverage of the film flow on the bottom wall can be achieved. These results are consistent with the studies reported in Ref[8].

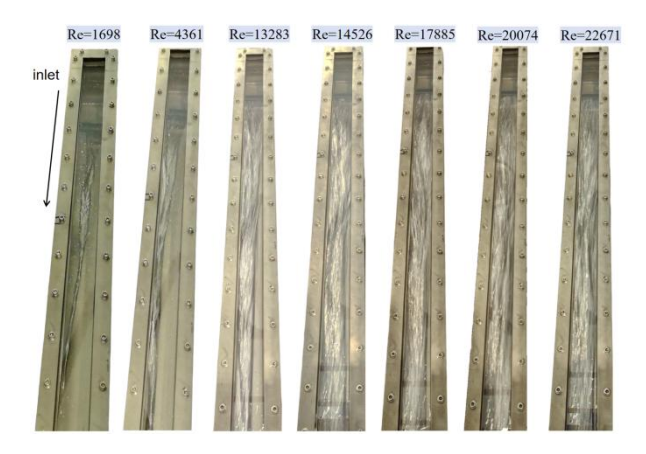


FIG. 3. Film flow pattern under different velocity (B=0T).

The influence of transverse magnetic field strength on the film flow spreading characteristics was investigated by applying the magnetic field strength from 0 to 1.8T along the spanwise direction, while keeping the GaInSn inlet velocity unchanged. The film flow patterns under different transverse magnetic field strength at a velocity of 0.433m/s are shown in FIG.4. In the presence of a magnetic field, the film surface flow gradually changes from a relatively disordered state (observed without a magnetic field) to a smoother state, indicating that magnetic fields suppress surface fluctuations. Moreover, stronger magnetic field exert greater suppression effects. This observed phenomenon is consistent with the findings in Ref. [19].



FIG. 4. Film flow pattern under different magnetic field strength (velocity=0.433m/s).

The film flow average thickness along the spanwise direction was measured at a distance of 350mm from the inlet. As shown in FIG.5, The film flow is in a turbulent state, with its surface fluctuating over time. The amplitude of fluctuations increases as the Reynolds number rises. Additionally, the average film thickness increases with an increasing Reynolds number.

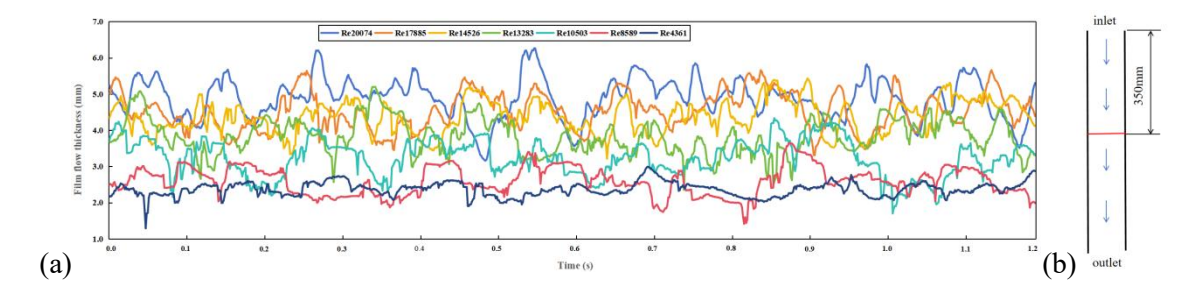


FIG. 5.(a) Film flow average thickness versus time at a distance of 350 mm from the inlet under different Reynolds numbers(B=0T); (b)Schematic Sketch of laser Scanning Line (red line).

The film flow thickness along the streamwise direction was measured and is presented in FIG.6. The results show that the film flow thickness tends to gradually increase from upstream to downstream. This phenomenon could be attributed to the continuous liquid supply at the inlet, coupled with blockage at the outlet downstream. As a result, the liquid film flow thickens along the streamwise direction due to mass accumulation, which is essentially a consequence of "inflow > outflow". The phenomenon of outlet blockage can be observed in FIG.4: near the outlet, the continuous accumulation of LM causes it to splash onto the upper glass cover plate. These observations suggest that optimization of the outlet design should be considered in future experiments.

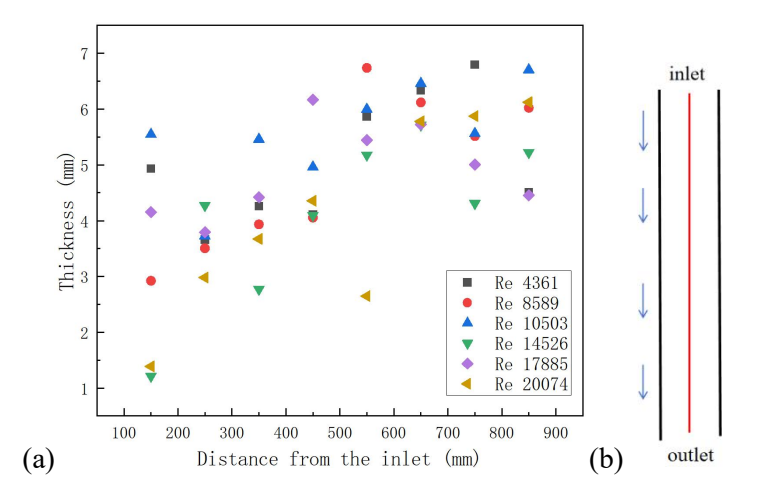


FIG. 6. (a) Film flow thickness along the spanwise direction under different Reynolds numbers (B=0T); (b) Schematic Sketch of Laser Scanning Line (red line).

### 3.2. Film flow simulation results

Film flow simulations were performed for the LM film flow under different Reynolds numbers, the results were compared with experimental data to validate their effectiveness. As shown in FIG.7, the simulation of the film flow simulation and experiment show good consistency. It should be noted that the contact angles between LM and the substrate material was assumed to be 135°, representing poor wettability. This assumption may introduce deviations from the experimental results due to discrepancies with the actual contact angle.

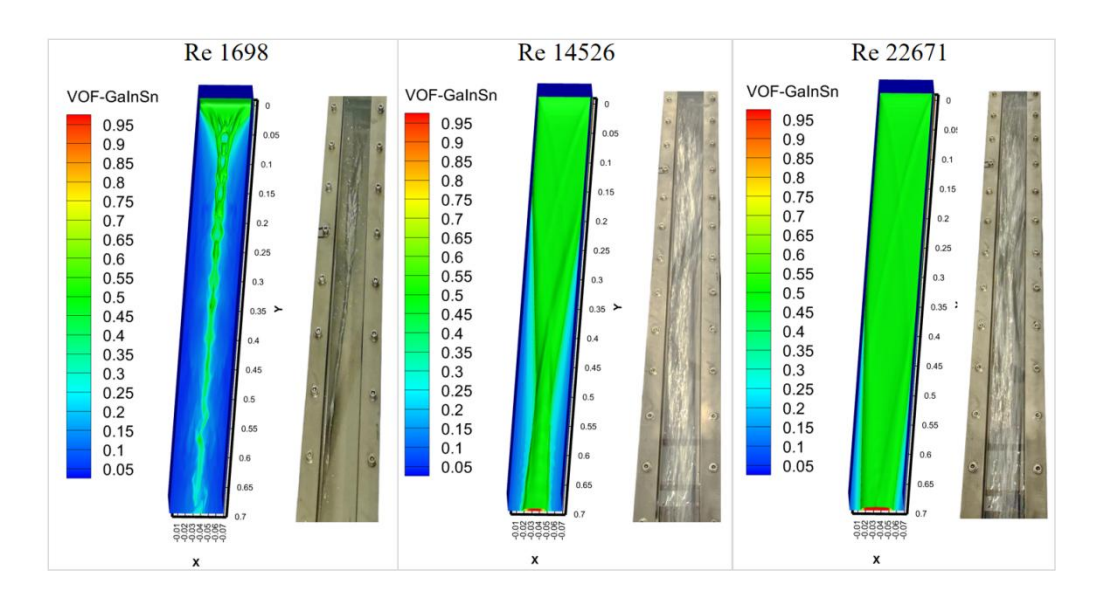


FIG. 7. Comparison between simulation and experimental results of GaInSn film flow under different flow velocities (B=0T).

FIG.8 illustrates the influence of chute angles on the film flow spreading characteristic, note the chute angle indicates  $\beta$  in FIG.1 and FIG.2. When the chute angle is  $0^{\circ}$  (placed horizontally), the LM flow is driven by the flow velocity. the LM cannot travel a long distance due to poor wettability; it reaches approximately 0.35 meters from the inlet before accumulating there. As the inclination angle increases, under the combined action of gravity and initial velocity, the spreading area of the film flow first increases and then decreases. The spreading area is the largest when the inclination angle is  $30^{\circ}$ . At  $90^{\circ}$ , the effect of gravity dominates, there is no sufficient time for the LM to spread on the bottom wall and instead flows downward under gravity, resulting in a reduced spreading area when reaching the downstream.

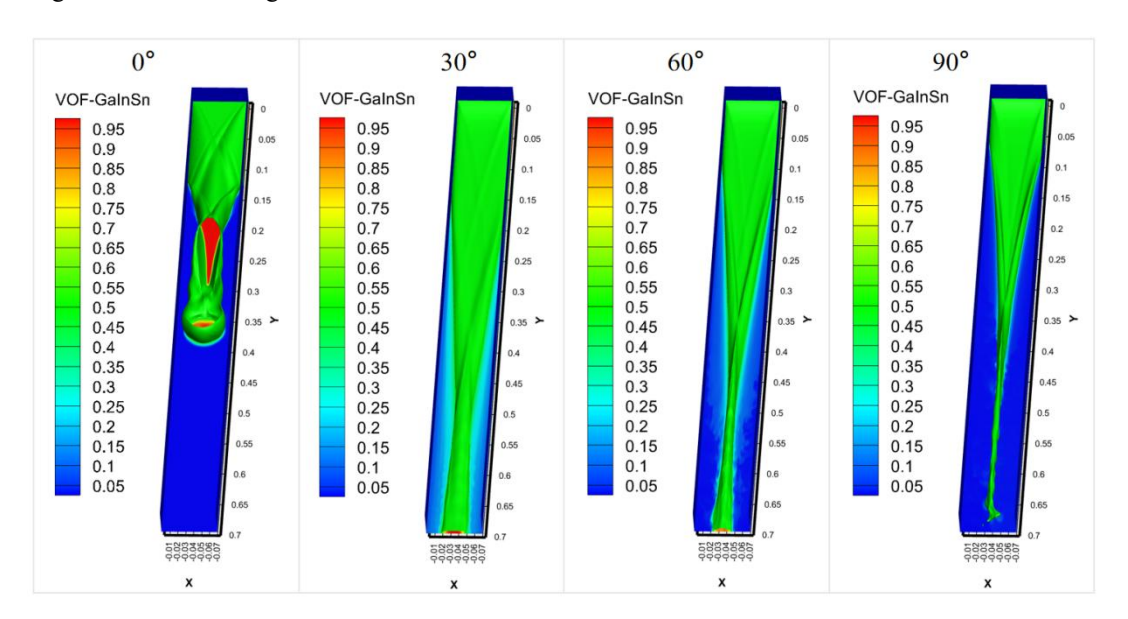


FIG. 8. Film flow characteristic under different chute angles (B=0T).

The above results indicate that it's difficult to achieve a stable and full-coverage film flow on a flat substrate material when Re<20000. To address this, two innovative bottom wall structure designs are proposed, aiming to realize the stable full coverage of the film flow through the optimization of the bottom wall structure. Both employ a sawtooth pattern aimed at enhancing flow stability and coverage. In proposal-1, the sawtooth is oriented along the streamwise direction, whereas in proposal-2 it is oriented along the spanwise direction, the details of sawtooth is shown in FIG.9. The concept of proposal-1 is that the LM can be temporarily retained in

the concave regions of the sawtooth-shaped structure, while proposal-2 is designed to guide and control the LM across the surface.

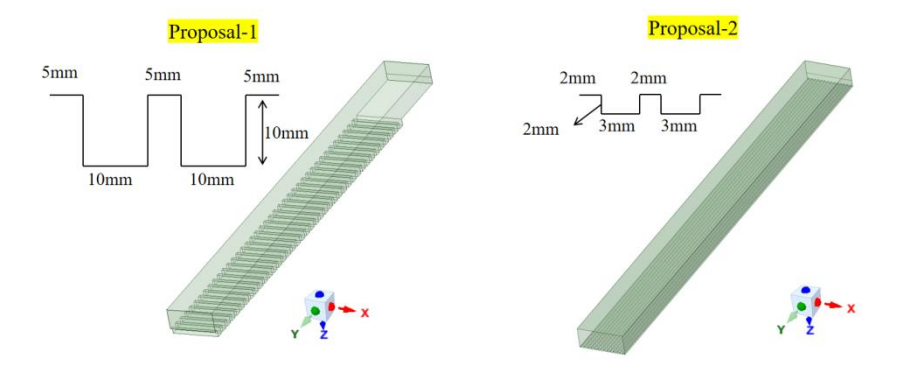


FIG. 9. Innovation structural proposals aiming at achieving full-coverage film flow.

Simulations were carried out under Re = 14526 and B = 0T for both proposed structured, with all boundary conditions kept identical. The chute angle was set to  $30^{\circ}$  and the contact angle was assumed to be  $135^{\circ}$ . The results are shown in FIG.10. Compared with the flat substrate, where full spreading occurs only up to  $\sim 200$  mm from the inlet, the bottom wall structure of Proposal-1 achieves full spreading up to  $\sim 450$  mm from the inlet. However, in the latter half of the film flow, detachment from the side walls still occurs, preventing complete coverage. Moreover, due to the sawtooth-shaped bottom wall structure, the flow fluctuations of GaInSn exhibit anisotropy. In contrast, Proposal-2, achieves nearly complete spreading, with only a small uncovered area near the outlet. This limitation could be mitigated through further structural optimization. Overall, both designs significantly increase the spreading area of the film flow, with Proposal 2 showing superior performance.

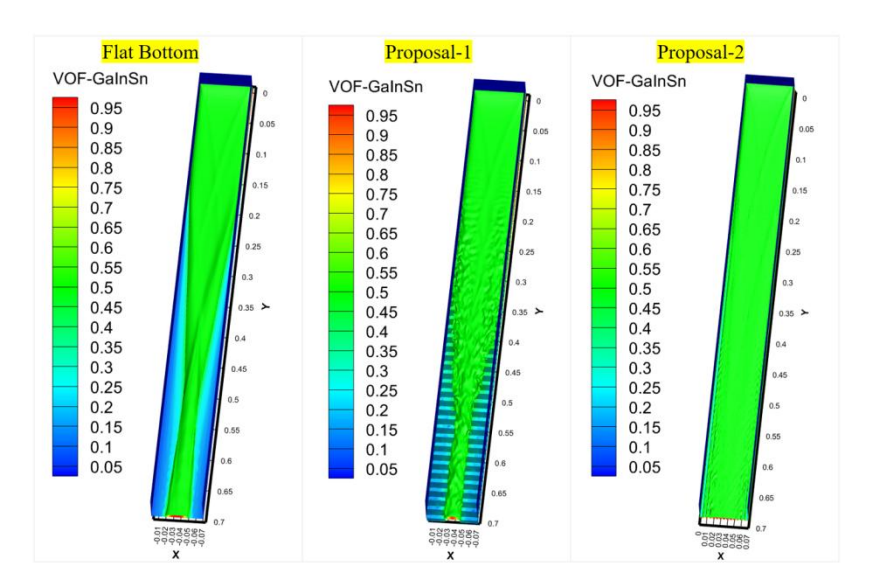


FIG. 10. Film flow simulation results of the innovation structural proposals compared with flat bottom(B=0T, Re=14526).

## 4. CONCLUSION

The following main conclusions are drawn from the numerical simulations and experimental investigations of GaInSn liquid metal film flow:

- (a) At constant transverse magnetic field strength, as the Re number increases, the spreading area and the average thickness of the film flow increase;
- (b) At constant Reynolds number, the film surface evolves from a relatively disorderly state (without a magnetic field) to a smoother state under magnetic field influence, demonstrating that magnetic fields suppress surface

waves. The suppression effect strengthens with increasing magnetic field intensity, and no significant obstruction of GaInSn film flow was observed;

- (c) The chute angle that maximizes film flow spreading is approximately 30°;
- (d) Preliminary full-coverage film flow without a magnetic field can be achieved through structural innovation. However, further researches is required to evaluate the spreading characteristics of the proposed bottom wall structure under magnetic fields.

#### REFERENCES

- [1] Andruczyk D, Maingi R, Kessel C, et al. A Domestic Program for Liquid Metal PFC Research in Fusion[J]. Journal of Fusion Energy, 2020:1-7.
- [2] J. Knaster, A. Moeslang, T. Muroga, Materials research for fusion, Nature Physics. 12 (5) (2016) 424-434.
- [3] Nagayama Y. Liquid lithium divertor system for fusion reactor[J]. FED, 2009, 84(7-11):1380-1383.
- [4] Goldston R J, Hakim A, Hammett G W, et al. Recent advances towards a lithium vapor box divertor[J]. Nuclear Materials & Energy, 2017:S235217911630103X.
- [5] Emdee E D, Goldston R J, Schwartz J A, et al. Study of lithium vapor flow in a detached divertor using DSMC code[J].Nuclear Materials & Energy, 2019, 19:244-249.
- [6] Stubbers R, Olczak W, Nieto M, et al. Measurement of hydrogen absorption in flowing liquid lithium in the flowing lithium retention experiment (FLIRE)[J]. Journal of Nuclear Materials, 2005, 337-339:1033-1037.
- [7] Smolentsev S, Rognlien T, Tillack M, et al. Integrated Liquid Metal Flowing First Wall and Open-Surface Divertor for Fusion Nuclear Science Facility: Concept, Design, and Analysis[J]. Fusion Science and Technology, 2019, 75(8):1-20.
- [8] Juan-Cheng Yang, Tian-Yu Qi, Ming-Jiu Ni, et al. Flow patterns of gainsn liquid on inclined stainless steel plate under a range of magnetic field. FED, 109:861–865, 2016.
- [9] JS Hu, GZ Zuo, J Ren, et al. First results of the use of a continuously flowing lithium limiter in high performance discharges in the east device. Nuclear Fusion, 56(4):046011, 2016.
- [10] P Rindt, SQ Korving, TW Morgan, et al. Performance of liquid-lithium-filled 3d-printed tungsten divertor targets under deuterium loading with elm-like pulses in magnumpsi. Nuclear Fusion, 61(6):066026, 2021.
- [11] Peter Rindt, J Mata Gonz alez, P Hoogerhuis, et al. Using 3d-printed tungsten to optimize liquid metal divertor targets for flow and thermal stresses. Nuclear Fusion, 59(5):054001, 2019.
- [12] Wang Y J, Li K L, Chen R Z, et al. Experimental investigation of a novel liquid metal plasma facing component with pre-filled microstructures [J]. 2025.
- [13] Anne-Marie Kietzig, Savvas G Hatzikiriakos, et al. Patterned superhydrophobic metallic surfaces. Langmuir, 25(8):4821–4827, 2009.
- [14] P Fiflis, A Press, W Xu, et al. Wetting properties of liquid lithium on select fusion relevant surfaces. Fusion Engineering and Design, 89(12):28272832, 2014.
- [15] SA Krat, AS Popkov, Yu M Gasparyan, et al. Wetting properties of liquid lithium on lithium compounds. Fusion Engineering and Design, 117:199–203, 2017.
- [16] Yang, Juan-Cheng, Tian-Yu, et al. Surface waves of liquid metal film flow under the influence of spanwise magnetic field[J]. Fusion Engineering and Design, 2018, 130:42-47.
- [17] Zhang X, Pan C, Xu Z. Experimental investigations on liquid metal MHD turbulent flows through a circular pipe with a conductive wall[J]. Fusion Engineering & Design, 2017, 125.